RSC Chemical Biology

ROYAL SOCIETY OF CHEMISTRY

PAPER

View Article Online
View Journal | View Issue

Cite this: *RSC Chem. Biol.*, 2026, 7, 105

Programmable synthesis of alkaloidal frameworks integrating Michael acceptor generates covalent probes for targeting POLE3 in HBV replication

Nobuto Kaneko,†[a] Misao Himeno,†[bc] Yuhi Kobayashi,[a] Ryo Tanifuji,[a] Hiroki Kubota,[d] Haruki Mizoguchi,[e] Makoto Muroi,[f] Takehiro Suzuki,[f] Masaya Sugiyama,[g] Naoshi Dohmae,*[f] Hiroyuki Osada,[f] Taketomo Kido,[c] Atsushi Miyajima*[c] and Hiroki Oguri*[a]

The growing need for effective HBV treatments and lead compounds with novel mechanisms prompted us to explore synthetic strategies for generating skeletally diverse alkaloidal Michael acceptors. Our approach uniquely embeds Michael acceptors directly within multicyclic alkaloid-inspired frameworks, exploiting the azepinoindole scaffold—a privileged structure in indole alkaloids. A single-step assembly between the versatile intermediate **13** with methyl propiolate **14** or its derivatives enabled the rapid and divergent synthesis of six alkaloidal Michael acceptors (**15**–**20**). This strategy facilitated systematic diversification of three-dimensional functional group arrangements and precise tuning of the electronic and steric properties of the embedded α,β-unsaturated carbonyl moieties. The optimal hit **15** inhibited hepatitis B surface antigen (HBsAg) production with an IC_{50} of 2.48 μM and significantly reduced levels of covalently closed circular DNA (cccDNA), the master template of HBV. Unlike existing nucleoside/nucleotide-based anti-HBV drugs that primarily inhibit reverse transcription, the alkaloidal Michael acceptor **15** suppressed both cccDNA and relaxed circular DNA (rcDNA) levels, suggesting a potential pathway toward a functional HBV cure. Our study also streamlined the target identification by leveraging the covalent binding properties of the Michael acceptors and the operational simplicity of biotin- or fluorescent-tag attachment *via* a pre-installed alkyne moiety. Competitive pull-down experiments identified several potential target proteins, involving DNA polymerase epsilon subunit 3 (POLE3). Notably, the alkaloidal Michael acceptor **15** was demonstrated to covalently modify Cys51 in POLE3, providing new insights into virus–host interactions and opening novel avenues for targeted anti-HBV therapies. This approach represents a significant advance beyond traditional screening methods and underscores the potential of skeletally diverse alkaloidal Michael acceptors in antiviral drug development.

Received 15th October 2025,
Accepted 18th October 2025

DOI: 10.1039/d5cb00268k

rsc.li/rsc-chembio

Introduction

Covalent modification of proteins with small molecules that bear electrophilic functional groups, such as Michael acceptors, is an effective strategy for drug development and the generation of chemical probes.[1] The hetero-conjugate addition between a thiol residue in a protein and a Michael acceptor functioning as a "warhead" in a small molecule ligand results in covalent adducts with high potency and prolonged effects on their target proteins.[2] Despite concerns of promiscuous bindings and potential off-target toxicity, there has been renewed interest in the therapeutic benefits of covalent modulators, which surpass those of conventional non-covalent inhibitors that interact with targets under equilibrium conditions.

In the last decade, there has been a significant increase in the number of covalent drugs that have been commercialized

[a] *Department of Chemistry, Graduate School of Science, The University of Tokyo, 7-3-1 Hongo, Bunkyo-ku, Tokyo 113-0033, Japan*
[b] *Department of Developmental Medical Sciences, Graduate School of Medicine, The University of Tokyo, 7-3-1 Hongo, Bunkyo-ku, Tokyo 113-0033, Japan*
[c] *Laboratory of Cell Growth and Differentiation, Institute for Quantitative Biosciences, The University of Tokyo, 1-1-1 Yayoi, Bunkyo-ku, Tokyo 113-0032, Japan*
[d] *Department of Applied Chemistry, Graduate School of Engineering, Tokyo University of Agriculture and Technology, 2-24-16 Nakacho, Koganei, Tokyo 184-8588, Japan*
[e] *Graduate School of Natural Science and Technology, Okayama University, 3-1-1 Tsushimanaka, Kita-ku, Okayama 700-8530, Japan*
[f] *Centre for Sustainable Resource Science, RIKEN, 2-1 Hirosawa, Wako, Saitama 351-0198, Japan*
[g] *Department of Viral Pathogenesis and Control, National Institute of Global Health and Medicine, Japan Institute for Health Security, 1-7-1 Kohnodai, Ichikawa City, Chiba 272-8516, Japan*
† The two authors N. K. and M. H. contributed equally.

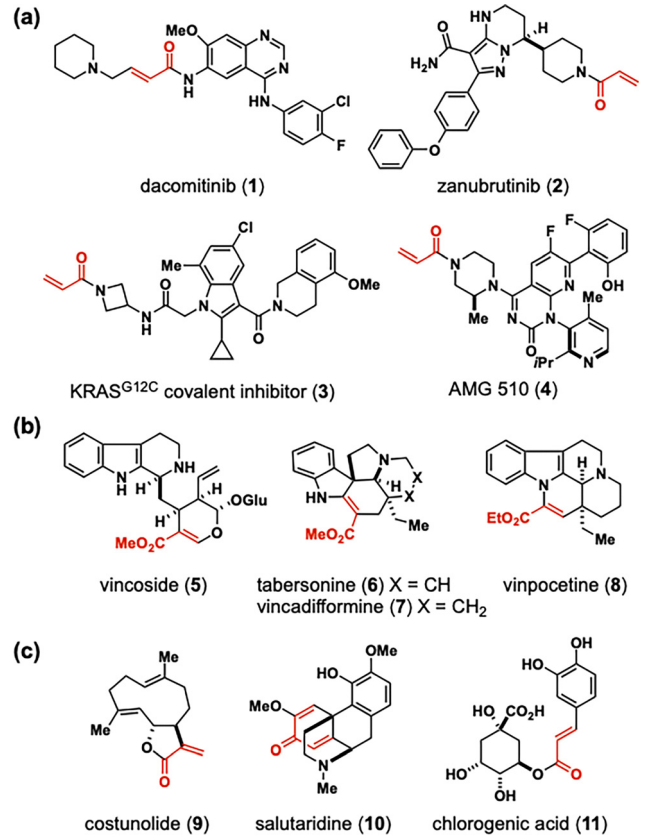

Fig. 1 (a) Recently approved covalent drugs and covalent inhibitors targeting KRAS. (b) Indole alkaloids **5–7** and semi-synthetic analogue **8** containing a Michael acceptor. (c) Natural products with α,β-unsaturated carbonyl groups exhibiting anti-HBV activity.

or are under clinical investigation.[3] Covalent inhibitors such as dacomitinib (**1**),[4] targeting the epidermal growth factor receptor (EGFR), and zanubrutinib (**2**),[5] targeting the Bruton's tyrosine kinase, were approved by the U.S. FDA in 2018 and 2019, respectively (Fig. 1a). In 2019, Amgen reported the development of an inhibitor **3** bearing an acrylamide-type Michael acceptor designed to form a covalent bond with the cysteine residue of the GTP-bound mutant KRASG12C.[6] This inhibitor was further structurally optimized to incorporate an axially chiral biaryl linkage, which increased the conformational rigidity of its heteroaromatic scaffold. This resulted in AMG 510 (**4**),[7] a highly potent and selective KRASG12C inhibitor, which was approved by the FDA in 2021 to treat non-small cell lung cancer.

Building on these precedents, we conceived a chemical-biology platform designed to strategically merge the covalent reactivity of Michael acceptors with the "privileged scaffold" of indole alkaloids (Fig. 1b). Unlike prevalent approaches, which typically rely on appending an α,β-unsaturated carbonyl moiety onto heterocyclic scaffolds as a terminal acrylamide-type substituent (Fig. 1a), we devised a design strategy that integrates the Michael acceptor "warhead" directly within a multicyclic alkaloidal framework (Fig. 2). In this study, we established a programmable synthetic platform based on a common azepinoindole intermediate **13**, enabling rapid and divergent generation of six distinct alkaloidal covalent probes (**15–20**) through an expeditious one-pot process. This skeletal-diversification strategy allows precise modulation of the three-dimensional architecture and both electronic and steric properties of the embedded Michael acceptor, thereby facilitating the generation of structurally and functionally diverse covalent small molecules.

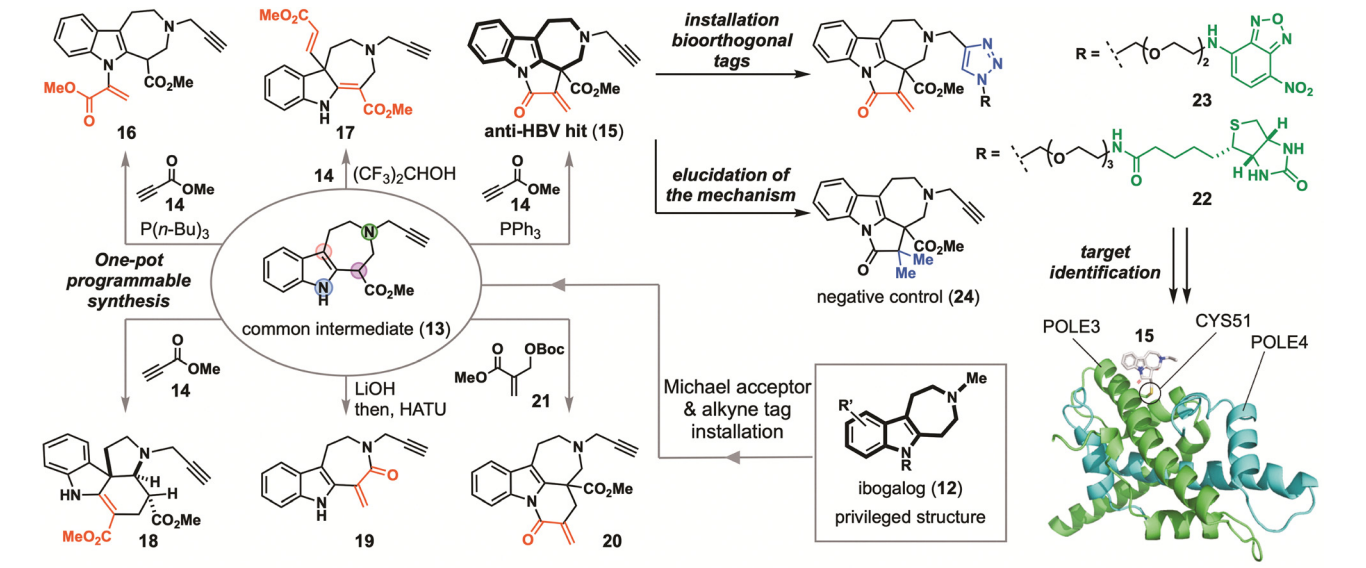

Fig. 2 Design of skeletally diverse alkaloidal Michael acceptors (**15–20**) based on the privileged scaffold **12**. A rapid, modular, and divergent synthetic process enabled the generation of pilot libraries for SAR studies on the anti-HBV hit compound **15**, as well as chemical probes (**22** and **23**) exploiting a preinstalled alkyne moiety for target identification. A working hypothesis for the formation of a covalent complex between **22** and a protein, along with its hydrogen-bonding networks.

Inspired by the natural products **9–11** bearing α,β-unsaturated carbonyl groups that exhibit antiviral activity against hepatitis B virus (HBV) (Fig. 1c), we designed and synthesized these skeletally diverse covalent probes (**15–20**) to identify potential antiviral hits (Fig. 2). Among them, the three covalent molecules (**15**, **16**, and **18**) exhibited pharmacological activity by suppressing (1) the secretion of HBV envelope protein hepatitis B surface antigen (HBsAg), (2) the accumulation of viral genomic relaxed circular DNA (rcDNA), and (3) the formation of covalently closed circular DNA (cccDNA).

This approach was designed to streamline target identification by leveraging the covalent binding capability of the identified hits and the operational simplicity offered by instant attachment of either a biotin or a fluorescent tag *via* a preinstalled alkyne moiety on the alkaloidal scaffold. We performed comparative and quantitative chemical proteomics experiments with HepAD38 cells, utilizing not only the biotin-tagged hit conjugate but also free ligand without the tag and a negative control lacking the Michael acceptor moiety. This strategy enabled the identification of potential target proteins and revealed that the optimal probe **15** covalently binds to Cys51 of DNA polymerase epsilon subunit 3 (POLE3), suggesting its potential role in modulating DNA polymerase function. This protein is presumed to regulate the cccDNA level, the master template of HBV replication. Therefore, this synthetic strategy based on natural product-inspired covalent probes provides a new avenue for designing small molecules with anti-HBV properties, potentially offering a functional cure for HBV infection.

Results and discussion

Design of skeletally diverse alkaloidal scaffolds bearing Michael acceptors as warheads

The secondary metabolisms of plants and microorganisms generate natural products that serve as rich resources for the covalent modifiers, exploiting the cellular reactivities of electrophilic warheads. Although numerous natural products bearing Michael acceptors have been identified in the terpenoid and polyphenol families (Fig. S20a and c), alkaloidal Michael acceptors remain relatively rare (Fig. 1b and Fig. S20b). While upstream biosynthetic intermediates of terpene indole alkaloids, such as secoiridoid glucoside vincoside (**5**), contain a Michael acceptor, the α,β-unsaturated carbonyl moieties are in most cases extensively manipulated during downstream biosynthetic processes to form alkaloidal scaffolds.[8] Consequently, alkaloids that retain a Michael acceptor, such as tabersonine (**6**) and vincadifformine (**7**),[9] represent a very small fraction of the vast diversity of naturally occurring alkaloids. Meanwhile, vinpocetine (**8**), a semi-synthetic derivative of the vinca alkaloid vincamine, is clinically used as a therapeutic agent for cerebrovascular disorders, including stroke and dementia, with minimal side effects or toxicity despite the presence of α,β-unsaturated carbonyl groups.[10]

A number of natural products containing Michael acceptors have been reported to exhibit antiviral activity (Fig. 1c). Costunolide (**9**), a well-known sesquiterpene lactone belonging to the germacranolide series, was isolated from *Saussurea lappa Clarke*.[11] It has various physiological activities such as antioxidant, anti-inflammatory, and neuroprotective effects, and has been shown to inhibit the expression of HBsAg in human hepatoma Hep3B cells and hepatitis B e antigen (HBeAg), a marker of hepatitis B virus genome replication, in human hepatoma and HepA2 cells. Salutaridine (**10**), a morphinian alkaloid isolated from *Corydalis saxicola* Bunting, has long been used clinically as a folk medicine to treat hepatitis and has been reported to inhibit HBsAg and HBeAg secretion in the HepG2.2.15 cell line.[12] Chlorogenic acid (**11**), an ester of quinic acid and caffeic acid, is a plant polyphenol widely found in coffee beans and other plants. It is known for its diverse antiviral activities and has been reported to suppress the replication of HBsAg and HBV DNA in HepG2.2.15 cells.[13]

Inspired by the intriguing yet underexplored biological potential of natural products containing α,β-unsaturated carbonyl groups and the promising pharmacological properties of alkaloidal scaffolds, we designed a series of alkaloidal Michael acceptors based on the azepino[4,5-*b*]indole, a privileged alkaloidal scaffold (Fig. 2). Recently, Olson *et al.* developed a non-hallucinogenic ibogalog (**12**) derived from the azepino-[4,5-*b*]indole scaffold, which exhibits anti-addictive and antidepressant activities through structural simplification and trimming of functional groups of a natural product, ibogaine.[14] By integrating the privileged alkaloidal scaffold ibogalog (**12**) with the pharmacophores of antiviral natural products possessing the cellular reactivities of electrophilic warheads (Fig. 1c), we envisioned a versatile synthetic strategy, featuring "chemical evolution" to generate high-hit rate screening collections. These synthetic small molecules that can be readily applied as covalent modulators and chemical probes to advance pharmaceutical and chemical biology research.

In this project, we designed a common intermediate **13** bearing a 6/5/7-membered tricyclic alkaloidal framework that contains both aliphatic and aromatic amino groups (Fig. 2). This key tricyclic intermediate **13** can be efficiently synthesized *via* modular assembly of three simple building blocks.[9b,15] This versatile intermediate **13** is designed to incorporate four nucleophilic sites: the indole N1 and C3 positions, the α-position of methyl ester, and an aliphatic tertiary amino group. To install a Michael acceptor and generate skeletal diversity into the alkaloidal scaffolds, we devised a site-selective addition of methyl propiolate **14**, at these four nucleophilic sites in a programmable manner, enabling the divergent synthesis of alkaloidal covalent binders **15–20** in a single-step process.

As shown in Fig. 2, the Michael addition of physiological thiols to **15** is expected to be essentially irreversible, and the stability of the resulting covalent adduct can be modulated through hydrogen bonding networks between adjacent residues and functional groups on the alkaloidal scaffold. By exploiting the pre-installed terminal alkynes of the alkaloidal scaffolds (**15–20**), the covalent adducts can be readily conjugated with biotins, fluorescent dyes, or other functional moieties for target identification and bioimaging applications.

Divergent synthesis of alkaloidal Michael acceptors

The versatile common intermediate **13** was readily synthesized from tryptamine in five steps.[9b,15] To begin, we designed a phosphine-catalysed nucleophilic addition of the indole nitrogen to the α-position of methyl propiolate **14** (Scheme 1).[16] The one-pot assembly of **13** with **14** in the presence of a catalytic amount of P(*n*-Bu)$_3$ (20 mol%) afforded **16** having an α-amino acrylate moiety in 50% yield. In addition, the tetracyclic Michael acceptor **15** having an *exo*-methylene γ-lactam with a quaternary carbon centre, was obtained as a minor product in 15% yield. The structures of both **15** and **16** were carefully elucidated by X-ray crystallographic analysis. Notably, the nucleophilic sites in **13** were different during its reaction with the electrophilic intermediates derived from **14**: the indole nitrogen participated in the formation of **16** as intended, whereas the α-position of ester in **13** was involved for **15**.

To improve the yield for the one-pot synthesis of the tetracyclic **15**, we found that replacing P(*n*-Bu)$_3$ with PPh$_3$ reversed the product ratios, ultimately increasing the isolated yield of **15** to 76% (Scheme 1). The use of molecular sieves 4A was crucial for achieving this improved yield of **15**. In the absence of molecular sieves, significant amounts of **16** having an α-amino acrylate moiety were predominantly formed instead.

These one-pot reactions likely involve the conjugate addition of phosphine to **14**, forming the zwitterionic intermediate **A** (Scheme 1).[16] This reactive intermediate **A** is thought to facilitate site-selective deprotonation at the most acidic proton, the indole N1 position, thereby generating an anionic species **B**. Under P(*n*-Bu)$_3$-mediated conditions, an N–C bond forming reaction between the resulting anion **B** and the cationic electrophile **C** would predominantly occur, leading to the formation of intermediate **D**. Subsequent deprotonation, followed by E1cB elimination from the corresponding enolate **E** could lead to the formation of product **16**.

Upon treatment with PPh$_3$, the initially formed zwitterionic intermediate **A** is in equilibrium with the cationic electrophile **C**. The PPh$_3$-derived electrophile **C** is considered to be more stabilised compared to its counterpart generated from P(*n*-Bu)$_3$. This increased stability suggests that the tautomerization of the intermediate **B** into the corresponding enolate **F** predominantly occurs prior to N–C bond formation with **B**. As a result, C–C bond formation between the enolate **F** and the cationic electrophile **C** is expected to proceed efficiently as the major pathway. Subsequent deprotonation of the indole NH group (**G** → **H**), followed by the intramolecular five-membered lactam formation, would generate intermediate **I**. Finally, an E1cB elimination from intermediate **I** would yield the tetracyclic Michael acceptor **15** as the major product.

Next, we investigated sequential reactions triggered by nucleophilic attack of the aliphatic tertiary amino group on the azepino[4,5-*b*]indole scaffold (Scheme 2). The ene–yne **25** was synthesized efficiently following a previously reported protocol.[9b] Upon treatment of **13** with methyl propiolate **14** in a mixed solvent (1,2-dichloroethane/trifluoroethanol = 1/1), conjugate addition of the tertiary amine to **14** generated the zwitterionic intermediate **J**. This intermediate underwent regioselective Hofmann elimination *via* deprotonation at the α-position of the methyl ester, resulting in the formation of ene–yne **25**, which simultaneously incorporated both a β-carbonyl enamine group and a vinyl indole moiety. The resulting intermediate **25**, containing two Michael acceptors, was then heated with triethylamine and hydroquinone in refluxing toluene, promoting an efficient intramolecular Diels–Alder type reaction *via* the *endo* transition state **K**. This cascade process furnished the tetracyclic alkaloidal scaffold **18** in 93% yield (2 steps from **13**), with the incorporation of a distinct β-carbonyl enamine group at the core of the tetracyclic framework.

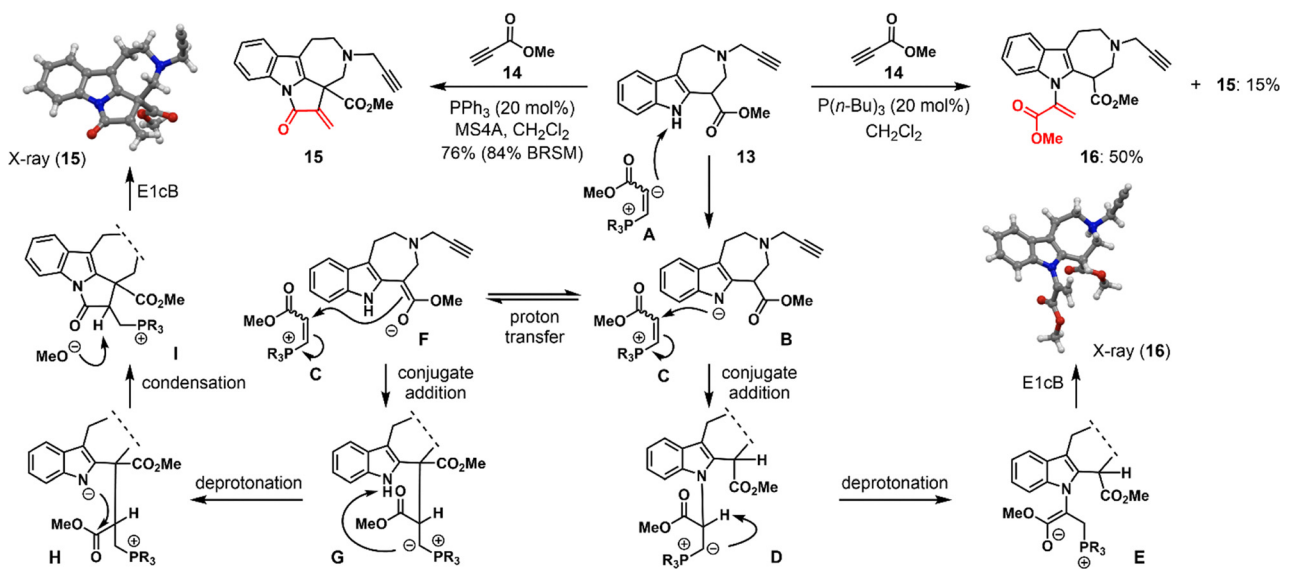

Scheme 1 Efficient one-pot synthesis of the Michael acceptors **15** with an *exo*-methylene γ-lactam and **16** with an α-amino acrylate unit. All compounds were synthesized as racemates.

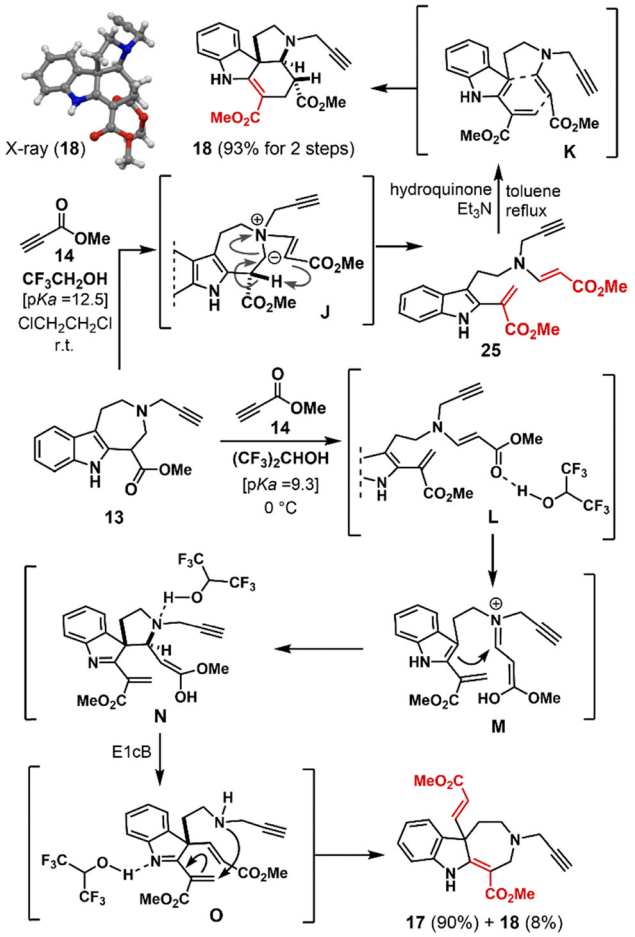

Scheme 2 Divergent synthesis of tetracyclic and tricyclic alkaloidal scaffolds **18** and **17** with installation of either one or two Michael acceptors, respectively. All compounds were synthesized as racemates.

The use of hexafluoro-2-propanol (HFIP)[17] in place of the trifluoroethanol[18] not only facilitated the assembly of **13** and **14**, but also triggered sequential one-pot transformations (Scheme 2). The conjugate addition/Hofmann elimination sequence proceeded as expected, even at 0 °C, generating ene–yne **25** in the presence of HFIP. Notably, subsequent intramolecular cascade reactions occurred under these conditions, which resulted in predominant formation of **17** which contains two Michael acceptors in 90% yield. A minor amount of the tetracycle **18** was also obtained as a byproduct in 8% yield. Although the yield of **18** was low under HFIP conditions, its formation indicates that the ene–yne **25** serves as an intermediate, undergoing a subsequent Diels–Alder reaction to furnish **18**. More importantly, the conversion of the ene–yne **25** into the tricycle **17** appears to be the predominant reaction, when HFIP was used as solvent. Indeed, treatment of ene–yne **25** with HFIP led to the formation of tricycle **17** in approximately 77% yield (see Page S10 for details). This yield was estimated based on NMR analysis using an internal standard method due to the labile nature of **25**.

Based on these experimental findings, we propose a plausible mechanism for the one-pot synthesis of tricyclic product **17** from **13** *via* ene–yne **25** (Scheme 2). In contrast to treatment with the mildly acidic trifluoroethanol [pK_a = 12.5], the stronger acidity of HFIP [pK_a = 9.3] facilitates protonation of the β-carbonyl enamine group in **25**, generating an electrophilic iminium cation (intermediate **L** → **M**). This cationic intermediate **M** likely induces a 5-*endo* cyclisation at the nucleophilic indole C3 position, forming the spirocyclic intermediate **N**. Protonation of the aliphatic amino group then promotes an E1cB-type elimination, resulting in the formation of an α,β-unsaturated ester moiety and ring-fission to yield intermediate **O**. A subsequent intramolecular hetero-conjugate addition furnishes the tricyclic product **17**, regenerating the seven-membered ring with installation of two Michael acceptors in good yield (90%). Notably, this one-pot sequence involves the migration of the methyl propiolate unit from the aliphatic amino nitrogen to the C3 position of the indole ring.

We then explored the possibility of site-selective *N*-acylation or conjugate addition at the α-position of the ester substituent to methyl propiolate **14**, aiming to form an endocyclic Michael acceptor **26** (Scheme 3). Although the desired product **26** was not obtained, treatment of **13** with NaH and **14** in DMF afforded spirocyclic pyridoindole **27** in 24% yield. This transformation is proposed to proceed *via* a β-elimination followed by an intramolecular vinylogous Mannich-type reaction. The crystalline structure of **27** was unambiguously confirmed by X-ray analysis.

This outcome is presumably attributed to the electron deficiency of the quaternary carbon in **26**, which is conjugated

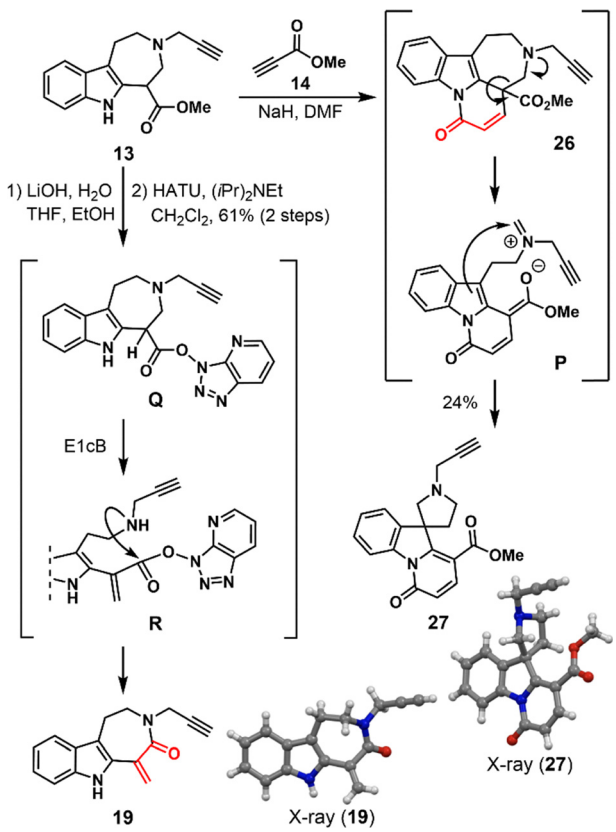

Scheme 3 Divergent synthesis of **27** (racemate) and **19**.

to the resulting Michael acceptor. This functional group arrangement likely induces ring scission of the seven membered azepino ring, generating iminium cation **P**, which subsequently undergoes intramolecular Mannich-type cyclization at the indole C3 position to form the spirocyclic pyridoindole **27**.

While developing this synthetic process for covalent ligands, we serendipitously found an interesting rearrangement reaction that enabled the efficient and operationally straightforward installation of an exocyclic double bond (Scheme 3). Hydrolysis of the methyl ester in **13** under basic conditions and subsequent treatment of the resulting carboxylic acid with HATU led to a rearrangement to produce **19** in good yield (61% for 2 steps). The structure of the tricyclic alkaloidal Michael acceptor **19** was unambiguously confirmed by X-ray analysis. Although the precise mechanism remains unidentified, it is presumed that the formation of activated ester **Q** facilitated an E1cB-type elimination to generate intermediate **R**. Subsequent intramolecular cyclisation between the resultant secondary amine and the activated ester would afford the seven membered lactam **19**. While there are several reports of the synthesis of the closely related *exo*-cyclic Michael acceptor based on the privileged azepino[4,5-*b*]indole scaffold,[19] this finding provides a streamlined and operationally simple protocol.

To achieve divergent synthesis of the variant **20**, composed of δ-lactam framework (Scheme 4), in place of the *exo*-methylene γ-lactam moiety in **15**, we devised an assembly strategy utilizing the common intermediate **13** with electrophiles **21**, applying the phosphine-catalyzed protocols developed by Kwon *et al.*[20] To construct the *exo*-methylene δ-lactam moiety in **20**, acrylic acid derivative **21** as the corresponding C4 segment was used, in place of **14**, to generate an allyl phosphonium species **S**. The subsequent assembly of intermediates **F** and **S**, followed by lactam formation *via* zwitterionic **T** and E1cb elimination was expected to install the *exo*-methylene functionality in the δ-lactam framework. As anticipated, the PPh_3-catalysed one-pot assembly of **13** with **21** proceeded smoothly at room temperature to afford **20** in 54% yield.

Thus, we have established a programmable one-pot process to access six distinct alkaloidal Michael acceptors (**15–20**) from the assembly of a common intermediate **13** and electrophiles, in which regioselectivity arising from multiple nucleophilic sites of **13** and the incoming electrophiles is precisely controlled through rational tuning of reaction conditions.

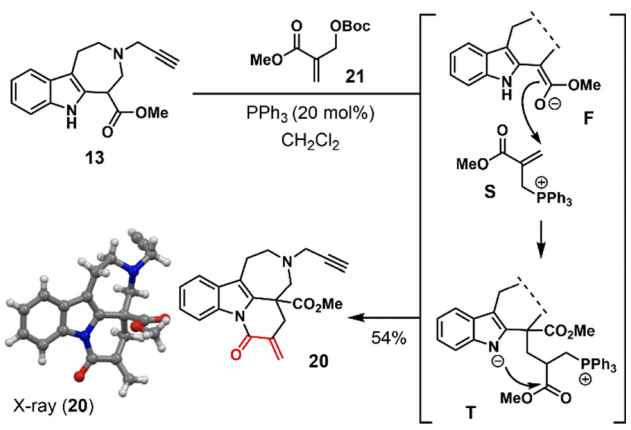

Scheme 4 Synthesis of **20** (racemate).

Inhibition of HBsAg secretion in HepAD38 cells

To evaluate the antiviral potential of the six alkaloid-inspired Michael acceptors (**15–20**), along with the natural product **6**, and a relevant semi-synthetic analog **8**, we assessed their activities against hepatitis B virus (HBV) replication using an *in vitro* assay employing HBV-replicating HepAD38 cells (Fig. 3a and b). In this cell line, the HBV genome is integrated under the transcriptional control of a tetracycline-regulated promoter.[21] The anti-HBV activity of each compound was evaluated by quantifying the secretion of hepatitis B surface antigen (HBsAg) into the culture supernatants using an enzyme-linked immunosorbent assay (ELISA). As shown in Table 1, five alkaloidal scaffolds—**15**, **16**, **18**, **19**, and **20**—each bearing a Michael acceptor moiety, exhibited potent and dose-dependent inhibition of HBsAg secretion, with IC_{50} values of 2.48, 1.34, 4.98, 3.16, and 1.99 μM, respectively (Table 1, entries 1, 2, 4–6 and Fig. S1–S4). In contrast, the other two alkaloidal Michael acceptors, **17** and **8**, showed negligible inhibitory effects (entries 3 and 8). Notably, while the natural product, tabersonine (**6**), shares the same tetracyclic substructure with the synthetic analog **18**, it exhibited only modest inhibitory activity, slightly weaker than that of **18** (entries 4 and 7). Furthermore, a negative control compound **24**, lacking the Michael acceptor moiety and instead bearing a *gem*-dimethyl derivative, showed negligible inhibition of HBsAg secretion at the same concentration (5 μM) (entry 9). These control experiments clearly underscore the crucial role of the α,β-unsaturated carbonyl group in mediating the observed anti-HBV activity of the five hit compounds **15**, **16**, **18**, **19**, and **20**.

Reduction of intracellular HBV rcDNA in HepAD38 cells

We subsequently evaluated the inhibitory effects of selected compounds (5 μM) on the intracellular levels of HBV partially double-stranded relaxed circular DNA (rcDNA) using quantitative PCR (qPCR) (Table 1).[22] Among the five hit compounds, Michael acceptors **15** and **16** exhibited substantial inhibitory activity, reducing rcDNA levels by ~66% and over 95%, respectively (entries 1 and 2). The tetracyclic **18**, possessing three consecutive sp^3 stereogenic centers, showed moderate but appreciable inhibition (approximately 30%, entry 4). In contrast, tricyclic **19** as well as tetracyclic **20**, exhibited only weak activity (approximately 10% inhibition, entries 5 and 6). Despite their close structural similarity and comparable inhibition of HBsAg secretion, **15** and **20** exerted markedly different effects on rcDNA levels. This observation implies that the subtle structural change from a five-membered γ-lactam in **15** (66% inhibition) to a six-membered δ-lactam in **20** (8.8% inhibition) exerts a profound influence on the molecular interactions with host or viral factors governing rcDNA processing. Consistent with their poor HBsAg inhibition, compounds **6**, **8** and **17** showed minimal or no effect on rcDNA reduction. These results

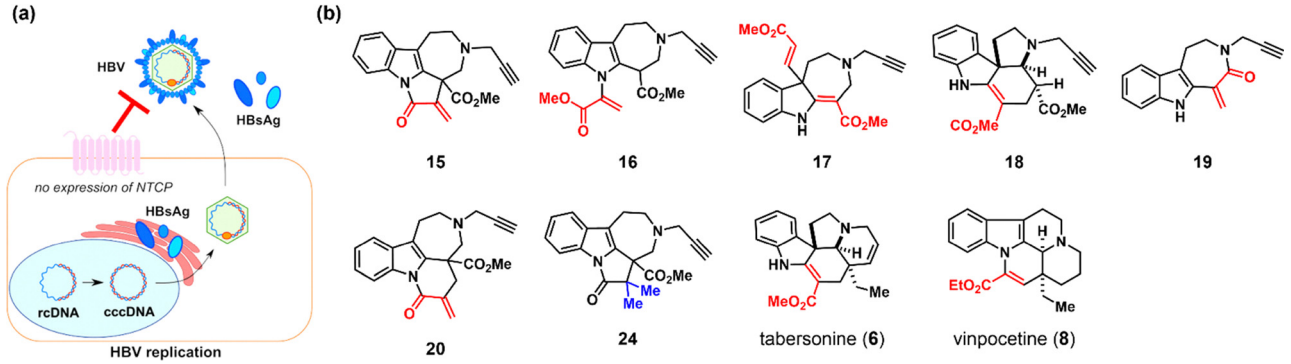

Fig. 3 Anti-viral effects of **15–20** in HBV-replicating HepAD38 cells. (a) HepAD38 cells integrated HBV genomes induced cccDNA-dependent HBV replication. (b) Structure of synthetic compounds (**15–20** and **24**), natural product **6**, and semisynthetic alkaloidal Michael acceptor **8**.

Table 1 The inhibitory effects of the synthetic compounds (**15–20**), natural product **6**, and semi-synthetic alkaloidal Michael acceptor **8** on HBsAg secretion and HBV rcDNA replication, as well as their cytotoxicity to HepAD38 cells, were evaluated in the range of 0 to 100 μM and are summarized

Entry	Compound	HBsAg IC_{50} [μM]	rcDNA inhibition [%]: compound (5 μM)	Cytotoxicity CC_{50} [μM]	Selectivity index: CC_{50}/IC_{50}
1	**15**	2.48 ± 0.33	66	13.7 ± 1.3	5.52
2	**16**	1.34 ± 0.06	>95	12.7 ± 0.76	9.48
3	**17**	n.a.	n.a.	>100	—
4	**18**	4.98 ± 3.41	30	>100	>20.1
5	**19**	3.16 ± 0.41	10	43.8 ± 1.7	13.9
6	**20**	1.99 ± 0.34	8.8	13.3 ± 1.8	6.68
7	**6**	14.6 ± 4.1	n.a.	41.8 ± 3.1	2.86
8	**8**	n.a.	n.a.	>100	—
9	**24**	n.a.	n.d.	>100	—

n.a.: negligible activity. n.d.: no data.

indicate that three compounds **15**, **16**, and **18** exert dual inhibitory effects by lowering both extracellular HBsAg and intracellular rcDNA levels in HepAD38 cells.

Assessment of cytotoxicity of hit compounds in HepAD38 cells

Small molecules possessing a Michael acceptor are often flagged as pan-assay interference compounds (PAINS), raising concerns about false positive effects and potential toxicity arising from assay interference or non-specific interactions.[23] To evaluate cytotoxicity of the hit compounds in HepAD38 cells, *in vitro* cell viability was assessed using an MTS assay across a concentration range of 0 to 100 μM (Table 1 and Fig. S2–S4). As a reference, the negative control **24**, which lacks the α,β-unsaturated carbonyl groups (entry 9), showed negligible cytotoxicity (CC_{50} > 100 μM). In addition, the three alkaloidal scaffolds **17**, **18**, and **8**, bearing either two or one Michael acceptor moieties (entries 3–4 and 8), exhibited minimal cytotoxicity (CC_{50} > 100 μM) toward HepAD38 cells, despite potential concerns regarding non-specific toxicity. The sterically demanding Michael acceptor **18**, consisting of a relatively electron-rich β-enaminocarbonyl moiety, exhibited no significant cytotoxicity even at 100 μM, whereas tabersonine (**6**) showed very weak cytotoxicity (CC_{50} 42 μM, entry 7). The tricyclic Michael acceptor **19**, bearing an exomethylene adjacent to the indole C2 position, also showed modest cytotoxicity (CC_{50} 44 μM, entry 5). Among the hit compounds, **16** with an α-substituted methylacrylate moiety, and **15** and **20**, each possessing an exomethylene group adjacent to a quaternary carbon centre within their α,β-unsaturated carbonyl systems on five- and six-membered rings, respectively, displayed modest cytotoxicity, with CC_{50} values approximately 13 μM (entries, 1, 2, 6 and Fig. S2, S3). For compound **S18** (see Page S14 for synthetic preparation), replacement of the *N*-propargyl group in **16** with an *N*-ethyl azide moiety, resulted in increased cytotoxicity (CC_{50}: 2.83 μM) while maintaining comparable inhibitory potency against HBsAg secretion (IC_{50}: 3.26 μM) in the HepAD38 cells (Fig. S6).

Conventional structure–activity relationship (SAR) studies typically rely on modifying substituents and functional groups on heteroaromatic sp^2-rich scaffolds. In contrast, our synthetic approach enables skeletal diversification of an alkaloidal scaffold, thus provides insights into both the pharmacophore and the reactivities of the embedded Michael acceptors. This strategy highlights nitrogen-containing scaffolds as a largely underexplored chemotype for the development of antiviral small molecules.

Inhibitory effects on HBV in HuH7 cells expressing NTCP

Based on their substantial inhibitory effects and low to moderate cytotoxicity on HBV-replicating HepAD38 cells, the three

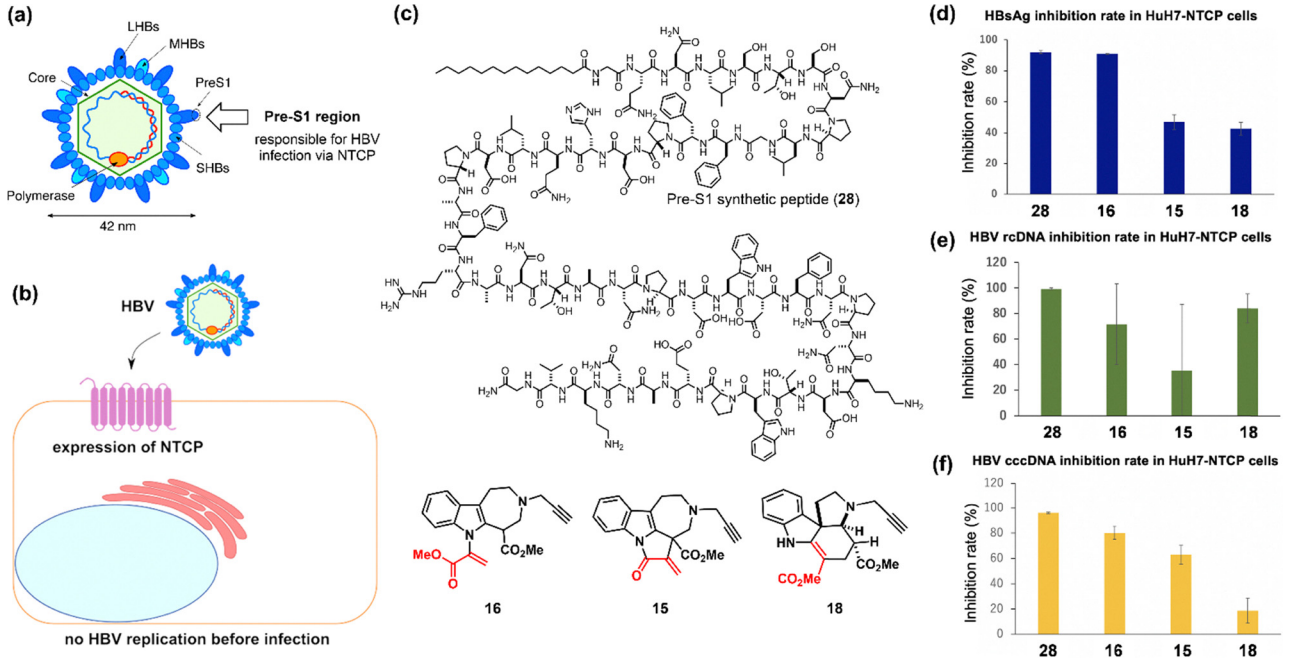

Fig. 4 Anti-viral effects of synthetic compounds (**15**, **16**, and **18**) and PreS1 synthetic peptide (**28**) employing an *in vitro* HuH7-NTCP HBV infection system. (a) The HBV particle is surrounded by a lipid bilayer and three envelope proteins, LHBs, MHBs and SHBs. Interaction of the PreS1 region of LHBs with the NTCP transporter plays a key role in HBV infection. (b) *In vitro* HBV infection model system with HuH7-NTCP cells that stably express the NTCP transporter responsible for the infection of HBV particles but not the integration of the HBV genome. There is no HBV replication in HuH7-NTCP cells before infection through the NTCP transporter expressed on the cell surface. (c) Structure of three alkaloidal Michael acceptors (**15**, **16**, and **18**) and PreS1 peptide (**28**: 100 nM), a myristoylated peptide consisting of the N-terminal 47 residues of the preS1 domain of the HBV L protein (LHBs). (d) Inhibitory effects of the three Michael acceptors (**15**, **16**, and **18**: 5 μM each) and PreS1 synthetic peptide (**28**: 100 nM) on HBsAg secretion. (e) Inhibitory effects of the three Michael acceptors (**15**, **16**, and **18**: 5 μM each) and PreS1 synthetic peptide (**28**: 100 nM) on the levels of rcDNA. (f) Inhibitory effects of the three Michael acceptors (**15**, **16**, and **18**: 5 μM each) and PreS1 synthetic peptide (**28**: 100 nM) on the levels of cccDNA.

hits (**15**, **16**, and **18**) were selected as optimal alkaloidal Michael acceptors. To assess *in vitro* anti-HBV efficacy of the hits against the processes involving both infection to the hepatocytes and virus replication in the host cells, we conducted further assays employing HuH7-NTCP cells that stably express human Na^+ taurocholate cotransporting polypeptide (NTCP) (Fig. 4a and b).[24] In this infection model, the inhibitory activities of the three compounds (**15**, **16**, and **18**) were assessed by the measuring levels of HBsAg, rcDNA, and cccDNA, and compared to a synthetic peptide (**28**: 100 nM). This peptide **28**, composed of an N-terminal glycine myristoylated 47 amino acid segment of the PreS1 domain of LHB protein, serves as a positive control that inhibits HBV infection *via* the NTCP transporter (Fig. 4c).[25]

The three optimal Michael acceptors (**15**, **16**, and **18**), each tested at 5 μM, demonstrated inhibitory activity by reducing HBsAg secretion from HuH7-NTCP cells, showing structure and activity relationships similar to those observed in HepAD38 cells (Fig. 4d). Compound **16** exhibited significant inhibitory activity (>90%), while compounds, **15** and **18**, resulted in moderate inhibitory effects, achieving 40–50% inhibition. Compounds **16** and **18** also demonstrated stronger inhibitory effects (>60%) on rcDNA levels in HuH7-NTCP cells compared to **15** (<40%) (Fig. 4e).

Based on these results, we further evaluated the pharmacological effects on the clearance of cccDNA, the master template for all seven viral proteins and other generator of four major RNA species, as well as the expression of the HBV outer shell component protein HBsAg, using qPCR analysis.[22] Notably, compound **16** exhibited substantial inhibitory activity (~80%) against the cccDNA level in HuH7-NTCP cells (Fig. 4f). Compound **15** also demonstrated substantial inhibitory activity (>60%), while **18** showed modest activity (~20%).

Following the observation that compounds **15**, **16**, and **18** effectively reduced cccDNA levels in HBV-infected HuH7-NTCP cells, we next evaluated their cytotoxicity under the same cellular conditions. Importantly, all three compounds exhibited minimal cytotoxicity, as determined by MTS assays at concentrations ranging from 0.1 to 5 μM (Fig. S10).

Selection of the optimal alkaloidal Michael acceptor

To evaluate the intrinsic electrophilicity of our scaffolds, we investigated the kinetics of thiol Michael addition for four representative compounds (**15**, **16**, **18**, and **19**) with glutathione as a cysteine surrogate in phosphate-buffered saline (PBS, pH 7.4) containing 5% DMSO at 37 °C (Fig. S8 and S9). The observed results are consistent with general principles of chemical reactivity. For example, the sluggish reaction observed for **18** aligns with the expected low reactivity of its sterically demanding and electron-rich β-enaminocarbonyl moiety. Likewise, the slow reaction of **19** is typical for acrylamide-type

systems, which are generally weaker Michael acceptors than esters. Surprisingly, the tetracyclic alkaloidal Michael acceptor **15**, having an *exo*-methylene γ-lactam, exhibited over 20-fold higher reactivity than the tricyclic **16**, which bears an α-substituted methylacrylate moiety. This was unexpected given the increased steric congestion around **15**, arising from the quaternary carbon center. Under the same conditions, the thiol additions to the two compounds **18** and **19** proceeded only sluggishly.

Although tricyclic **16** exhibited slightly higher anti-HBV activity in cellular assays, its slow reaction kinetics with glutathione suggested inefficient covalent modification of its ultimate protein target, making it less suited for reliable proteomic capture. In contrast, tetracyclic **15** combines two favorable features—an embedded α,β-unsaturated carbonyl and steric constraint from the quaternary centre—resulting in substantially higher intrinsic electrophilicity while retaining significant biological activity. For chemical proteomic profiling, **15** was therefore selected as the representative alkaloidal Michael acceptor, as it offered an optimal balance between cellular potency and electrophilic reactivity, enabling efficient and selective covalent labeling of nucleophilic protein residues.

Having established **15** as the most suitable scaffold for target identification, we next explored how structural modification impacts antiviral activity. To this end, six derivatives (**S2**–**S5**, **S7**, **S8**) were designed and synthesized (Schemes S1 and S2), incorporating systematic modifications of the tetracyclic scaffold of **15**. These included an ethyl ester derivative (**S2**), a methoxy analogue (**S3**), two trisubstituted olefins derived from the exomethylene unit (**S4** and **S5**), and two *N*-propargyl replacements with bulkier groups (**S7** and **S8**). When evaluated at 5 μM in HepAD38 cells, none of these analogues surpassed **15** in suppressing HBsAg secretion (Fig. S1) or reducing rcDNA levels (Fig. S7). These results suggest that the selected covalent probe **15** possesses a finely tuned balance between electrophilicity and biological potency, which seems essential for its antiviral activity. Accordingly, **15** was retained as the probe molecule for subsequent target identification studies.

Initial pull-down experiments using HepAD38 cells

We initially conducted conventional streptavidin pull-down experiments by synthesizing conjugate **22**, in which alkaloidal Michael acceptor **15** was linked to a biotin unit *via* click chemistry (for synthetic details, see page S16). Exploiting the preinstalled *N*-propargyl group on **15**, copper(I)-catalyzed azide–alkyne cycloaddition (CuAAC) with commercially available biotin-PEG3-azide afforded the biotinylated probe **22**.[26] Upon incubating HepAD38 cell lysate with the biotin-tagged **22**, the covalently bound proteins were captured using streptavidin-agarose beads, separated by SDS–PAGE, and subsequently analyzed by LC-MS/MS (Fig. S12 and Table S1). However, due to the inherently promiscuous reactivity of the small molecule Michael acceptors, the detection of multiple covalently modified proteins posed substantial challenges in narrowing down the primary target proteins based on this conventional pull-down approach.

Competitive pull-down experiments against HepAD38 cells

To identify the specific target proteins while excluding non-specific or non-covalent binders, we performed competition assays using the three ligands: the hit compound **15**, its biotin conjugate **22**, and the negative control **24** (Fig. 5).[27] The negative control lacks the Michael acceptor moiety and instead bears a *gem*-dimethyl group at the α-position of the Michael acceptor in **22**.

In method A, biotin conjugate **22** was incubated with HepAD38 cell lysates and subjected to pull-down with streptavidin-coated beads, enabling the comprehensive capture of both covalent and non-covalent binders. In method B, the lysate was pretreated with the non-biotinylated compound **15** before the addition of the biotin conjugate **22**, allowing us to identify specific targets as proteins whose enrichment was reduced by competition with **15** (red peaks), thereby indicating specific covalent target engagement. In method C, pretreatment with **24** instead of **15** served as a negative control to identify proteins (blue peaks) that bind nonspecifically to

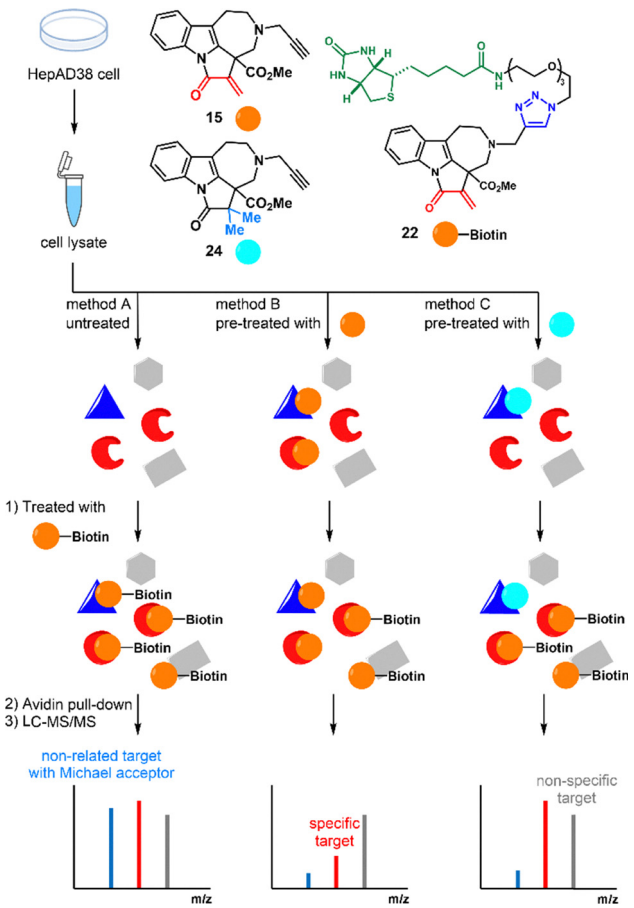

Fig. 5 Target identification of the alkaloidal Michael acceptor **15**. Schematic illustration of the competitive and quantitative pull-down experiments. HepAD38 cell lysates were treated with either DMSO, hit compound **15** (250 μM), and a negative control **24** (250 μM). These samples were then exposed with biotin-tagged conjugate **22** (25 μM). The resultant covalent adducts were captured with streptavidin-agarose, thoroughly washed, digested and analyzed by LC-MS/MS.

Table 2 Four proteins as plausible targets for hit compound **15**. Four proteins relevant to HBV treatments showed specific affinity to pretreated **15** with the peak intensity ratio of less than 0.2 (method B/A). In contrast, pretreatment with a negative control **24** resulted in negligible changes with the peak intensity ratio close to 1.0 (method C/A)

Protein	Relative ratio (method B/A)	Relative ratio (method C/A)
Vitamin K epoxide reductase 1 (VKORC1)	0.028	1.000
Isoform 2 of F-box only protein 38 (FBXO38)	0.141	0.914
Arfaptin-1 (ARFIP1)	0.158	1.000
Subunit 3 of DNA polymerase ε (POLE3)	0.196	1.017

structural regions other than the Michael acceptor moiety. Together, these comparative experiments enabled the identification of covalently modified proteins while filtering out non-covalent binders or nonspecific interactors.

Based on these competitive and quantitative pull-down experiments (Fig. 5 and Fig. S13), we successfully narrowed down potential target proteins that exhibited a significant reduction—to less than one-fifth of their initial amounts in the LC-MS peaks—while showing almost no change when preincubated with the negative control **24** (Table S2). From the short-listed proteins (Table 2), we focused on the four candidates as target proteins involved in the anti-HBV effects of hit compound **15**: vitamin K epoxide reductase 1 (VKORC1), isoform 2 of F-box only protein 38 (FBXO38), arfaptin-1, and subunit 3 of DNA polymerase epsilon (Pol ε).

Incubation of four candidate proteins with fluorescence-labelled probe 23

Among the ten proteins identified through competitive pull-down experiments (Table S2), we selected those that would not be membrane-bound for expression. Of the six proteins chosen, three—subunit 3 of DNA polymerase epsilon (POLE3), arfaptin-1 (ARFIP1), and isoform 2 of F-box only protein 38 (FBXO38)—were successfully expressed as N-His tagged proteins and subsequently purified. In addition, commercially available vitamin K epoxide reductase 1 (VKORC1) tagged with an N-GST, was included in this study. These four proteins were incubated with increasing concentrations of a fluorescent-labeled probe **23**. Fluorescent bands corresponding to subunit 3 of Pol ε (Fig. 6a), ARFIP1, and isoform 2 of FBXO38 were detected in a dose-dependent manner (Fig. S14), whereas VKORC1 showed no detectable signal.

Identification of the covalent binding site of 15 in POLE3

Having established experimental evidence supporting the interaction between the fluorescence-labelled probe **23** with the three target proteins (Fig. S14), we performed trypsin digestion followed by LC-MS/MS analysis to identify the specific amino acid residues involved in the covalent bond formation with the hit compound **15**. While attempts to identify binding sites in ARFIP1 and isoform 2 of FBXO38 proved challenging, covalent binding of **15** successfully detected POLE3. The analysis

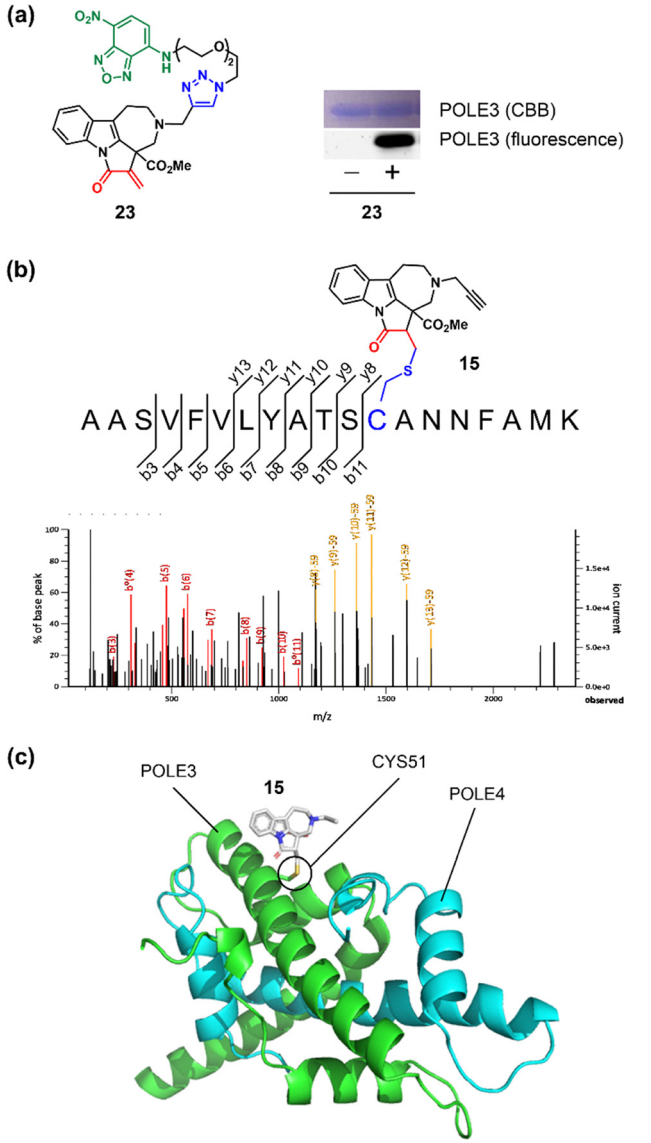

Fig. 6 Hit compound **15** and the fluorescently labeled derivative **23** form a covalent bond with cysteine residues of the target protein POLE3. (a) Structure of NBD conjugated hit compound **23** and Labelling of POLE3 with **23**, CBB staining (top) fluorescence (bottom). (b) LC-MS/MS analysis of **15** bound peptide fragments by peptide digestion. (c) Predicted structure of POLE3/4 complex by ColabFold and location of Cys51 binding with **15**.

revealed covalent adducts of **15** with cysteine-containing peptide fragments, and subsequent fragmentation pattern analysis identified Cys51 in POLE3 as the primary modification site (Fig. 6b). Tandem mass spectrometry confirmed peptide sequence coverage through a series of b- and y-ions. The detection of diagnostic fragment ions further confirmed the covalent modification. Additionally, LC-MS/MS analysis revealed two distinct peaks corresponding to diastereomers of the covalent adduct derived from **15**, indicating comparable reactivity of both enantiomers in the racemic mixture (Fig. S15). These findings suggest that each enantiomer of **15** covalently modifies POLE3 at Cys51 with similar efficiency.

Covalent docking simulation with 15 and POLE3

We performed covalent docking simulations of the hit compound **15** with DNA polymerase epsilon subunit 3 (POLE3) (Fig. 6c). In DNA polymerase epsilon, subunits POLE3 and POLE4 are known to form a tight complex that contributes to histone binding and nucleosome assembly.[28] Although the crystal structure of human POLE has not been elucidated, it shares high homology with yeast POLE complex.[29] Therefore, the structure of the POLE3–POLE4 complex was predicted using ColabFold Multimer[30] based on the yeast Dpb3–Dpb4 complex (PDB: 5Y26).[31] The predicted model displayed high structural similarity to the yeast complex, validating its suitability for subsequent docking studies.

Covalent docking was performed using GNINA 1.3,[32] targeting a covalent bond between the α,β-unsaturated carbonyl moiety of **15** and Cys51 of POLE3. The lowest-energy docked structure was further refined using LigandScout 4.5[33] to optimize ligand conformation and the orientation of surrounding residues. Docking simulations of the four possible stereoisomers of **15** (Fig. S17), differing at the quaternary carbon bearing the methyl ester and the α-carbonyl chiral centre, revealed that the (*R*,*R*) or (*S*,*S*)-isomers configurations formed more extensive multipoint hydrogen-bonding networks with surrounding residues (Tyr47, Ser50, and Asn54) than the (*R*,*S*) and (*S*,*R*)-isomers. Notably, the methyl ester group of **15** was consistently observed to form a hydrogen bond with Asn54.

Discussion on the role of DNA polymerase inhibition in reducing HBV cccDNA levels

Persistent HBV infection promotes liver cirrhosis and hepatocellular carcinoma, posing major health threats to nearly 300 million individuals worldwide.[34] As illustrated in Fig. 7, the life cycle of HBV is initiated by viral particle entry into a hepatocyte and ends with the secretion of newly produced HBV out of the infected cell (for additional description for the HBV life cycle, see Page S43–S44 and Fig. S19).[35] To cope with global HBV infection rates, there is growing demand for the development of novel drugs with mechanisms of action distinct from existing nucleoside/nucleotide analogues (NAs) (Fig. S21).[35] Since NAs inhibit the reverse transcription step for the nascent nucleocapsid, the generation of newly formed viral DNA and viral particles from viral pre-genomic RNA (pg RNA) can be efficiently suppressed. NAs have thus been the cornerstone of chemotherapy in chronic HBV patients; however, NA-based drugs inevitably entail the emergence of drug resistance and

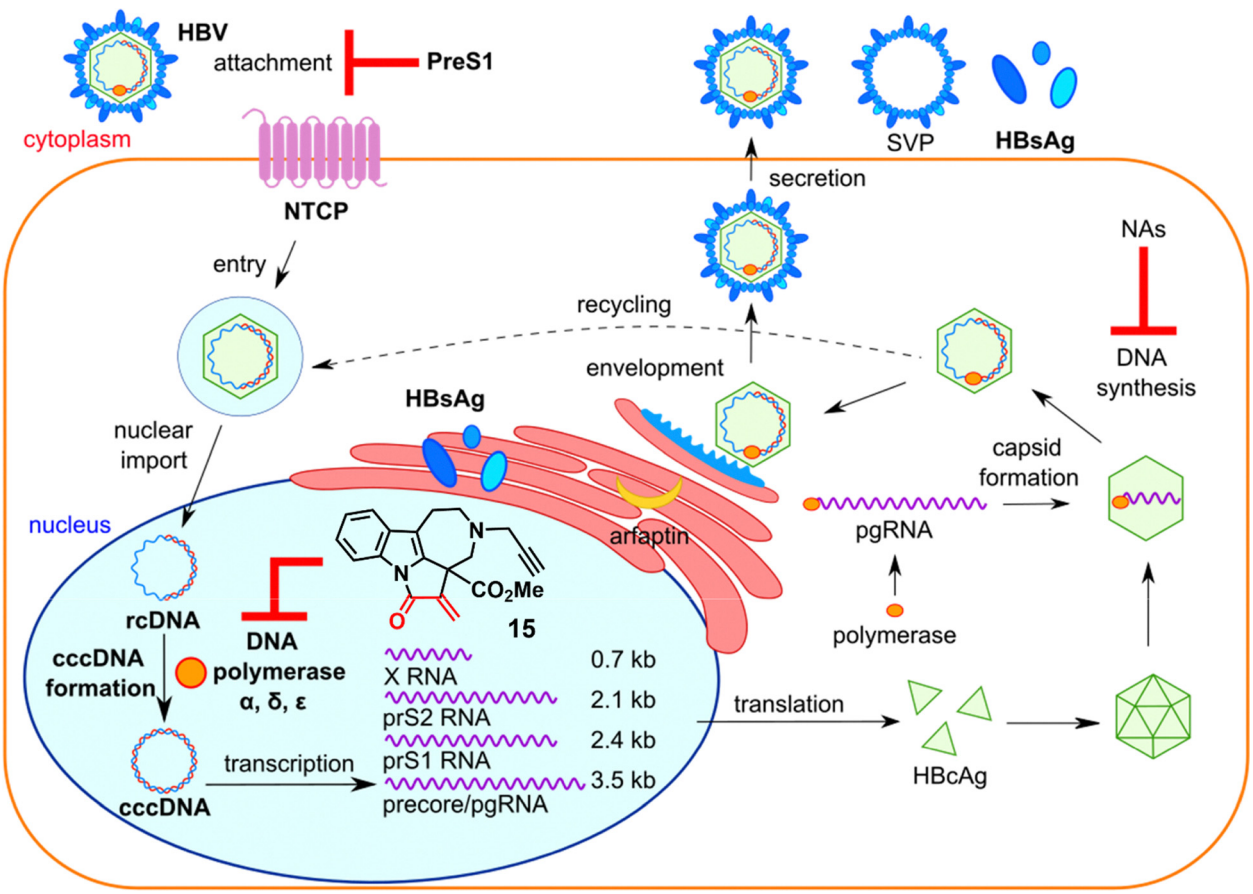

Fig. 7 Schematic illustration of the HBV life cycle with the mode of action of nucleoside/nucleotide analogues (NAs) and a plausible mechanism of action for the optimal alkaloidal Michael acceptor **15**. HBV, hepatitis B virus; HBsAg, hepatitis B virus surface antigen; NTCP, sodium taurocholate cotransporting polypeptide; pgRNA, pregenomic RNA; rcDNA, relaxed circular DNA; cccDNA, covalently closed circular DNA; SVP, subviral particle.

safety concerns, especially for long-term use.[36] More importantly, NAs are in principle unable to suppress the production of the four kinds of viral RNAs and viral proteins derived from cccDNA.

HBV cccDNA is reported to be stably maintained within an infected hepatocyte, albeit in minor amounts, and could serve as the master template for all viral transcription and protein synthesis.[31] Elimination and/or silence of HBV cccDNA could be a promising therapeutic strategy leading to eradication of the virus and complete cure of hepatitis.[37] In addition to the critical importance of cccDNA clearance, it is generally believed that the elimination of hepatitis B virus surface antigen (HBsAg) secretion will lead to a ''functional cure'' of chronic hepatitis B, as HBsAg is a key protein responsible for the pathogenesis of HBV infection and correlates with the prevalence of intrahepatic cccDNA levels.[38]

Recent work by Guo and colleagues has demonstrated that DNA polymerases alpha (Pol α), delta (Pol δ), and epsilon (Pol ε) are crucial for rcDNA-to-cccDNA conversion in HepAD38 cells, as evidenced by gene knockdown experiments using siRNA.[39] In line with these findings, aphidicolin, a known inhibitor of these polymerases, effectively reduces cccDNA levels in a dose-dependent manner (1–10 μM) in HepAD38 cells, underscoring its potential to impede HBV replication. These results from both genetic and chemical genetic investigations indicate that inhibition of these DNA polymerases can effectively reduce cccDNA levels, underscoring the therapeutic potential of targeting these polymerases.[39]

This study demonstrates that the alkaloidal Michael acceptor **15** covalently binds to Cys51 of DNA polymerase ε subunit 3 (POLE3). POLE3 typically forms a complex with its partner subunit POLE4, and our docking simulations suggest that the binding of **15** to Cys51 sterically clashes with the helical region of the POLE4. This implies that compound **15** may interfere with the formation of the POLE3–POLE4 complex. These findings are consistent with the established role of replicative DNA polymerases, particularly Pol α, Pol δ, and Pol ε, in the conversion of rcDNA to cccDNA (Fig. S14).[40] Consistently, both aphidicolin and the alkaloidal Michael acceptor **15** markedly reduce cccDNA levels, presumably through inhibition of these DNA polymerases. However, a major challenge associated with small-molecule polymerase inhibitors lies in their potential cytotoxicity, highlighting the need to develop analogs or combinatorial approaches that retain antiviral potency while minimizing host toxicity.

Discussion on the role of the other three detected proteins

As discussed above, the covalent binding of the alkaloidal Michael acceptor **15** to Cys51 of POLE3 provides a compelling hypothesis for the effective reduction of HBV cccDNA levels. This hypothesis is consistent with previous findings on aphidicolin, a known DNA polymerase inhibitor, reinforcing its mechanistic plausibility. In contrast, the identification of binding sites for the other three candidate proteins—FBXO38, arfaptin-1, and VKORC1—remains experimentally challenging.

Currently, little is known about the role of FBXO38, an E3 ubiquitin ligase, in HBV-related protein degradation.[41] Arfaptin-1, a BAR domain-containing protein, may contribute to the biogenesis of secretory granules or nuclear trafficking of HBV through the *trans*-Golgi network,[42] as depicted in Fig. 7, suggesting that pharmacological targeting of this pathway could influence HBV entry and intracellular trafficking dynamics. Meanwhile, VKORC1, a key regulator of vitamin K metabolism,[43] may influence HBV replication through redox regulation, with VKORC1 inhibitors such as dicoumarol emerging as potential antiviral candidates.[44] In light of these findings, further studies are required to elucidate the functional roles of these proteins in HBV pathogenesis. The identification of novel host-directed antiviral strategies, particularly those targeting DNA polymerases and host cellular factors, may open new therapeutic avenues and help overcome resistance to current HBV treatments.

Conclusion

In conclusion, this study demonstrates the effectiveness of a scaffold and reactivity diversification strategy for covalent ligand discovery. The programmable generation of six distinct alkaloidal frameworks (**15–20**) from a common intermediate **13** enabled the rapid identification of a tetracyclic Michael acceptor **15** exhibiting a unique anti-HBV activity profile. This optimal covalent probe **15** effectively reduced viral rcDNA and cccDNA levels while inhibiting HBsAg protein secretion (IC_{50}: 2.48 μM for HepAD38 cells) with modest cytotoxicity (CC_{50}: 13.7 μM). By leveraging the intrinsic covalent reactivity of the embedded Michael acceptor and enabling facile conjugation with either a biotin or fluorescent moiety *via* a preinstalled terminal alkyne, we performed competitive and quantitative pull-down experiments. The strategic use of three complementary molecules—**15**, its negative control **24**, and the biotinylated conjugate **22**—significantly narrowed down the potential host proteins involved in HBV replication. Subsequent trypsin digestion and LC-MS/MS analysis of the covalent adducts identified Cys51 of POLE3 as the binding site for **15**. The design and synthesis of skeletally diverse alkaloidal Michael acceptors has provided novel insights into the virus–host protein interactions. This versatile synthetic platform not only advances our understanding of viral replication mechanisms, but also provides a broadly applicable framework for targeted antiviral and chemical-biology probe development, underscoring the utility of this divergent synthetic approach for covalent ligand discovery across diverse biological systems.

Our findings further demonstrate that skeletally diverse natural product analogues, bearing both nitrogen-containing fused scaffolds and electrophilic functional groups capable of covalent modification, represent a promising paradigm for antiviral small molecule discovery in the absence of prior target knowledge. In contrast to conventional medicinal approaches that primarily simplify complex natural products, our strategy expands the landscape of lead-generation by complementing existing pharmaceutical and therapeutic modalities.

Author contributions

H. Oguri, N. K. and M. H. designed the research and H. Oguri led the team. N. K., H. K., and H. M. performed the chemical experiments and analyzed the data. M. H. evaluated the anti-HBV activity and cytotoxicity, and M. H., M. S., T. K., and A. M. analyzed the data. M. M. and T. S. performed proteomic profiling, and N. K., M. H., R. T., and M. M. performed protein expression and pull-down experiments with feedback from N. D. and H. Osada, N. K., M. H., A. M., and H. Oguri wrote the manuscript with feedback from all authors.

Conflicts of interest

The authors declare no competing financial interest.

Data availability

All data supporting the findings of this study are available within the article and its supplementary information (SI). Supplementary information: Synthetic procedures with full characterization data of compounds including NMR spectra, protocols for evaluation of anti-HBV activities and cytotoxicity, and X-ray crystal details for compounds. See DOI: **https://doi.org/10.1039/d5cb00268k**.

CCDC 2179523 (**15**), 2179524 (**16**), 2179775 (**18**), 2179518 (**19**), 2466308 (**20**), 2466313 (**27**) and 2466307 (**S5**) contain the supplementary crystallographic data for this paper.[45a–g]

Acknowledgements

We are grateful to Prof. Keiichi Noguchi (Tokyo Univ. of Agriculture and Technology) for X-ray analysis. The authors thank Prof. Hideaki Oikawa and Soushi Fujikawa (Hokkaido Univ.) as well as Mana Moriguchi and Shun Oyadomari (Tokyo Univ. of Agriculture and Technology) for preliminary synthetic studies and valuable discussions. This work was partially supported by JSPS KAKENHI (19H02847, 22H00346, and 22H05127), the Naito Foundation, and the Asahi Glass Foundation (H. O.). N. K. is grateful to the Program for Fostering Advanced Human Resources to Lead Green Transformation (SPRING GX). This work was inspired by the international and interdisciplinary environments of the JSPS Asian CORE Program, ''Asian Chemical Biology Initiative'', and JSPS A3 Foresight Program.

Notes and references

1 (*a*) J. Singh, R. C. Petter, T. A. Baillie and A. Whitty, *Nat. Rev. Drug Discovery*, 2011, **10**, 307–317; (*b*) R. A. Bauer, *Drug Discovery Today*, 2015, **20**, 1061–1073; (*c*) M. Gehringer and S. A. Laufer, *J. Med. Chem.*, 2019, **62**, 5673–5724; (*d*) S. Ray and A. S. Murkin, *Biochemistry*, 2019, **58**, 5234–5244; (*e*) H. Kim, Y. S. Hwang, M. Kim and S. B. Park, *RSC Med. Chem.*, 2021, **12**, 1037–1045.

2 (*a*) P. A. Jackson, J. C. Widen, D. A. Harki and K. M. Brummond, *J. Med. Chem.*, 2017, **60**, 839–885; (*b*) G. Wu, T. Zhao, D. Kang, J. Zhang, Y. Song, V. Namasivayam, J. Kongsted, C. Pannecouque, E. De Clercq, V. Poongavanam, X. Liu and P. Zhan, *J. Med. Chem.*, 2019, **62**, 9375–9414.

3 F. Sutanto, M. Konstantinidou and A. Domling, *RSC Med. Chem.*, 2020, **11**, 876–884.

4 O. Kalous, D. Conklin, A. J. Desai, N. A. O'Brien, C. Ginther, L. Anderson, D. J. Cohen, C. D. Britten, I. Taylor, J. G. Christensen, D. J. Slamon and R. S. Finn, *Mol. Cancer Ther.*, 2012, **11**, 1978–1987.

5 Y. Guo, Y. Liu, N. Hu, D. Yu, C. Zhou, G. Shi, B. Zhang, M. Wei, J. Liu, L. Luo, Z. Tang, H. Song, Y. Guo, X. Liu, D. Su, S. Zhang, X. Song, X. Zhou, Y. Hong, S. Chen, Z. Cheng, S. Young, Q. Wei, H. Wang, Q. Wang, L. Lv, F. Wang, H. Xu, H. Sun, H. Xing, N. Li, W. Zhang, Z. Wang, G. Liu, Z. Sun, D. Zhou, W. Li, L. Liu, L. Wang and Z. Wang, *J. Med. Chem.*, 2019, **62**, 7923–7940.

6 Y. Shin, J. W. Jeong, R. P. Wurz, P. Achanta, T. Arvedson, M. D. Bartberger, I. D. G. Campuzano, R. Fucini, S. K. Hansen, J. Ingersoll, J. S. Iwig, J. R. Lipford, V. Ma, D. J. Kopecky, J. McCarter, T. San Miguel, C. Mohr, S. Sabet, A. Y. Saiki, A. Sawayama, S. Sethofer, C. M. Tegley, L. P. Volak, K. Yang, B. A. Lanman, D. A. Erlanson and V. J. Cee, *ACS Med. Chem. Lett.*, 2019, **10**, 1302–1308.

7 B. A. Lanman, J. R. Allen, J. G. Allen, A. K. Amegadzie, K. S. Ashton, S. K. Booker, J. J. Chen, N. Chen, M. J. Frohn, G. Goodman, D. J. Kopecky, L. Liu, P. Lopez, J. D. Low, V. Ma, A. E. Minatti, T. T. Nguyen, N. Nishimura, A. J. Pickrell, A. B. Reed, Y. Shin, A. C. Siegmund, N. A. Tamayo, C. M. Tegley, M. C. Walton, H. L. Wang, R. P. Wurz, M. Xue, K. C. Yang, P. Achanta, M. D. Bartberger, J. Canon, L. S. Hollis, J. D. McCarter, C. Mohr, K. Rex, A. Y. Saiki, T. San Miguel, L. P. Volak, K. H. Wang, D. A. Whittington, S. G. Zech, J. R. Lipford and V. J. Cee, *J. Med. Chem.*, 2020, **63**, 52–65.

8 (*a*) S. E. O'Connor and J. J. Maresh, *Nat. Prod. Rep.*, 2006, **23**, 532–547; (*b*) R. Tanifuji, A. Minami, H. Oguri and H. Oikawa, *Nat. Prod. Rep.*, 2020, **37**, 1098–1121.

9 (*a*) S. Zhao, G. Sirasani and R. B. Andrade, *Alkaloids: Chem. Biol. Perspect.*, 2021, **86**, 1–143; (*b*) H. Mizoguchi, H. Oikawa and H. Oguri, *Nat. Chem.*, 2014, **6**, 57–64; (*c*) O. Wagnieres, Z. Xu, Q. Wang and J. Zhu, *J. Am. Chem. Soc.*, 2014, **136**, 15102–15108.

10 Y. S. Zhang, J. D. Li and C. Yan, *Eur. J. Pharmacol.*, 2018, **819**, 30–34.

11 H. C. Chen, C. K. Chou, S. D. Lee, J. C. Wang and S. F. Yeh, *Antiviral Res.*, 1995, **27**, 99–109.

12 Y. R. Wu, Y. B. Ma, Y. X. Zhao, S. Y. Yao, J. Zhou, Y. Zhou and J. J. Chen, *Planta Med.*, 2007, **73**, 787–791.

13 Y. Zhao, C. A. Geng, Y. B. Ma, X. Y. Huang, H. Chen, T. W. Cao, K. He, H. Wang, X. M. Zhang and J. J. Chen, *J. Ethnopharmacol.*, 2014, **156**, 147–154.

14 L. P. Cameron, R. J. Tombari, J. Lu, A. J. Pell, Z. Q. Hurley, Y. Ehinger, M. V. Vargas, M. N. McCarroll, J. C. Taylor, D. Myers-Turnbull, T. Liu, B. Yaghoobi, L. J. Laskowski, E. I. Anderson, G. Zhang, J. Viswanathan, B. M. Brown,

M. Tjia, L. E. Dunlap, Z. T. Rabow, O. Fiehn, H. Wulff, J. D. McCorvy, P. J. Lein, D. Kokel, D. Ron, J. Peters, Y. Zuo and D. E. Olson, *Nature*, 2021, **589**, 474–479.

15 (*a*) P. Chen, L. Cao and C. Li, *J. Org. Chem.*, 2009, **74**, 7533–7535; (*b*) G. Tay, S. Nishimura and H. Oguri, *Chem. Sci.*, 2024, **15**, 15599–15609; (*c*) K. Shimohata, M. Moriguchi, M. Satake and H. Oguri, *ACS Catal.*, 2025, **13**, 10991–11002.

16 (*a*) I. Yavari and H. Norouzi-Arasi, *Phosphorus, Sulfur Silicon Relat. Elem.*, 2002, **177**, 87–92; (*b*) X. Chen, C. M. Au, P. Fang, Y. Xue, K. C. Leung and W. L. Chan, *Org. Lett.*, 2025, **27**, 5081–5086.

17 (*a*) I. Colomer, A. E. R. Chamberlain, M. B. Haughey and T. J. Donohoe, *Nat. Rev. Chem.*, 2017, **1**, 0088; (*b*) V. Pozhydaiev, M. Power, V. Gandon, J. Moran and D. Leboeuf, *Chem. Commun.*, 2020, **56**, 11548–11564.

18 D. Bonnet-Delpon, J.-P. Bégué and B. Crousse, *Synlett*, 2004, 18–29.

19 (*a*) C. Ferrer, C. H. Amijs and A. M. Echavarren, *Chem. – Eur. J.*, 2007, **13**, 1358–1373; (*b*) V. A. Peshkov, O. P. Pereshivko and E. V. V. D. Eycken, *Adv. Synth. Catal.*, 2012, **354**, 2841–2848; (*c*) M. Juárez-Calderón, D. M. Aparicio, D. Gnecco, J. R. Juárez, L. Orea, A. Mendoza, F. Sartillo-Piscil, E. del Olmo and J. L. Terán, *Tetrahedron Lett.*, 2013, **54**, 2729–2732; (*d*) K. Prasad and J. Nidhiry, *Synlett*, 2014, 2585–2590; (*e*) S. Yorimoto, A. Tsubouchi, H. Mizoguchi, H. Oikawa, Y. Tsunekawa, T. Ichino, S. Maeda and H. Oguri, *Chem. Sci.*, 2019, **10**, 5686–5698.

20 Y. C. Fan and O. Kwon, *Chem. Commun.*, 2013, **49**, 11588.

21 S. K. Ladner, M. J. Otto, C. S. Barker, K. Zaifert, G. H. Wang, J. T. Guo, C. Seeger and R. W. King, *Antimicrob. Agents Chemother.*, 1997, **41**, 1715–1720.

22 S. W. Chen, M. Himeno, Y. Koui, M. Sugiyama, H. Nishitsuji, M. Mizokami, K. Shimotohno, A. Miyajima and T. Kido, *Sci. Rep.*, 2020, **10**, 14349.

23 (*a*) J. B. Baell and G. A. Holloway, *J. Med. Chem.*, 2010, **53**, 2719–2740; (*b*) J. Baell and M. A. Walters, *Nature*, 2014, **513**, 481–483; (*c*) J. B. Baell and J. W. M. Nissink, *ACS Chem. Biol.*, 2018, **13**, 36–44.

24 (*a*) D. Witt-Kehati, M. Bitton Alaluf and A. Shlomai, *Viruses*, 2016, **8**, 21; (*b*) R. Xu, P. Hu, Y. Li, A. Tian, J. Li and C. Zhu, *Virol. J.*, 2021, **18**, 105.

25 (*a*) P. Gripon, I. Cannie and S. Urban, *J. Virol.*, 2005, **79**, 1613–1622; (*b*) S. Urban, R. Bartenschlager, R. Kubitz and F. Zoulim, *Gastroenterology*, 2014, **147**, 48–64.

26 (*a*) P. Thirumurugan, D. Matosiuk and K. Jozwiak, *Chem. Rev.*, 2013, **113**, 4905–4979; (*b*) E. F. Ruivo, L. M. Goncalves, L. A. Carvalho, R. C. Guedes, S. Hofbauer, J. A. Brito, M. Archer, R. Moreira and S. D. Lucas, *ChemMedChem*, 2016, **11**, 2037–2042.

27 (*a*) X. Chen, Y. Wang, N. Ma, J. Tian, Y. Shao, B. Zhu, Y. K. Wong, Z. Liang, C. Zou and J. Wang, *Signal Transduction Targeted Ther.*, 2020, **5**, 72; (*b*) C. X. Liu, Q. Q. Yin, H. C. Zhou, Y. L. Wu, J. X. Pu, L. Xia, W. Liu, X. Huang, T. Jiang, M. X. Wu, L. C. He, Y. X. Zhao, X. L. Wang, W. L. Xiao, H. Z. Chen, Q. Zhao, A. W. Zhou, L. S. Wang, H. D. Sun and G. Q. Chen, *Nat. Chem. Biol.*, 2012, **8**, 486–493.

28 C. Wang, J. Huang, Y. Li, J. Zhang, C. He, T. Li, D. Jiang, A. Dong, H. Ma, G. P. Copenhaver and Y. Wang, *Proc. Natl. Acad. Sci. U. S. A.*, 2022, **119**, e2213540119.

29 Y. Li, H. Asahara, V. S. Patel, S. Zhou and S. Linn, *J. Biol. Chem.*, 1997, **272**, 32337–32344.

30 (*a*) M. Mirdita, K. Schutze, Y. Moriwaki, L. Heo, S. Ovchinnikov and M. Steinegger, *Nat. Methods*, 2022, **19**, 679–682; (*b*) M. Baek, F. DiMaio, I. Anishchenko, J. Dauparas, S. Ovchinnikov, G. R. Lee, J. Wang, Q. Cong, L. N. Kinch, R. D. Schaeffer, C. Millan, H. Park, C. Adams, C. R. Glassman, A. DeGiovanni, J. H. Pereira, A. V. Rodrigues, A. A. van Dijk, A. C. Ebrecht, D. J. Opperman, T. Sagmeister, C. Buhlheller, T. Pavkov-Keller, M. K. Rathinaswamy, U. Dalwadi, C. K. Yip, J. E. Burke, K. C. Garcia, N. V. Grishin, P. D. Adams, R. J. Read and D. Baker, *Science*, 2021, **373**, 871–876; (*c*) R. Evans, M. O'Neill, A. Pritzel, N. Antropova, A. Senior, T. Green, A. Žídek, R. Bates, S. Blackwell, J. Yim, O. Ronneberger, S. Bodenstein, M. Zielinski, A. Bridgland, A. Potapenko, A. Cowie, K. Tunyasuvunakool, R. Jain, E. Clancy, P. Kohli, J. Jumper and D. Hassabis, *bioRxiv,* 2022, preprint, DOI: **10.1101/2021.10.04.463034**.

31 H. He, Y. Li, Q. Dong, A. Y. Chang, F. Gao, Z. Chi, M. Su, F. Zhang, H. Ban, R. Martienssen, Y. H. Chen and F. Li, *Proc. Natl. Acad. Sci. U. S. A.*, 2017, **114**, 12524–12529.

32 (*a*) A. T. McNutt, P. Francoeur, R. Aggarwal, T. Masuda, R. Meli, M. Ragoza, J. Sunseri and D. R. Koes, *J. Cheminf.*, 2021, **13**, 43; (*b*) A. T. McNutt, Y. Li, R. Meli, R. Aggarwal and D. R. Koes, *J. Cheminf.*, 2025, **17**, 28.

33 G. Wolber and T. Langer, *J. Chem. Inf. Model.*, 2005, **45**, 160–169.

34 WHO, *Hepatitis B Fact Sheet*, 2021.

35 (*a*) Y. Pei, C. Wang, S. F. Yan and G. Liu, *J. Med. Chem.*, 2017, **60**, 6461–6479; (*b*) S. Feng, L. Gao, X. Han, T. Hu, Y. Hu, H. Liu, A. W. Thomas, Z. Yan, S. Yang, J. A. T. Young, H. Yun, W. Zhu and H. C. Shen, *ACS Infect. Dis.*, 2018, **4**, 257–277; (*c*) S. Tsukuda and K. Watashi, *Antiviral Res.*, 2020, **182**, 104925.

36 (*a*) F. Zoulim and S. Locarnini, *Gastroenterology*, 2009, **137**, 1593–1608; (*b*) K. H. Kim, N. D. Kim and B. L. Seong, *Molecules*, 2010, **15**, 5878–5908; (*c*) Y. Ma, E. Frutos-Beltran, D. Kang, C. Pannecouque, E. De Clercq, L. Menendez-Arias, X. Liu and P. Zhan, *Chem. Soc. Rev.*, 2021, **50**, 4514–4540.

37 (*a*) F. Zoulim, *J. Hepatol.*, 2005, **42**, 302–308; (*b*) M. Levrero, T. Pollicino, J. Petersen, L. Belloni, G. Raimondo and M. Dandri, *J. Hepatol.*, 2009, **51**, 581–592; (*c*) R. Kapoor and S. Kottilil, *Future Virol.*, 2014, **9**, 565–585.

38 (*a*) E. Hadziyannis, D. Vassilopoulos and S. J. Hadziyannis, *Curr. Hepat. Rep.*, 2009, **8**, 169–172; (*b*) H. L. Chan, A. Thompson, M. Martinot-Peignoux, T. Piratvisuth, M. Cornberg, M. R. Brunetto, H. L. Tillmann, J. H. Kao, J. D. Jia, H. Wedemeyer, S. Locarnini, H. L. Janssen and P. Marcellin, *J. Hepatol.*, 2011, **55**, 1121–1131; (*c*) M. Cornberg, V. W. Wong, S. Locarnini, M. Brunetto, H. L. A. Janssen and H. L. Chan, *J. Hepatol.*, 2017, **66**, 398–411.

39 L. Tang, M. Sheraz, M. McGrane, J. Chang and J. T. Guo, *PLoS Pathog.*, 2019, **15**, e1007742.

40 L. Wei and A. Ploss, *Viruses*, 2021, **13**, 1463.
41 Y. Miao, S. Wang, J. Zhang, H. Liu, C. Zhang, S. Jin and D. Bai, *Med. Oncol.*, 2024, **41**, 178.
42 H. Gehart, A. Goginashvili, R. Beck, J. Morvan, E. Erbs, I. Formentini, M. A. De Matteis, Y. Schwab, F. T. Wieland and R. Ricci, *Dev. Cell*, 2012, **23**, 756–768.
43 W. D. Van Horn, *Crit. Rev. Biochem. Mol. Biol.*, 2013, **48**, 357–372.
44 F. Takeuchi, S. Ikeda, Y. Tsukamoto, Y. Iwasawa, C. Qihao, Y. Otakaki, R. Ryota, W.-L. Yao, R. Narita, H. Makoto, K. Watashi, T. Wakita, K. Takeuchi, K. Chayama, A. Kogure, H. Kato and T. Fujita, *PLoS One*, 2019, **14**, e0212233.
45 (*a*) CCDC 2179523: Experimental Crystal Structure Determination, 2025, DOI: **10.5517/ccdc.csd.cc2c4z6q**; (*b*) CCDC 2179524: Experimental Crystal Structure Determination, 2025, DOI: **10.5517/ccdc.csd.cc2c4z7r**; (*c*) CCDC 2179775: Experimental Crystal Structure Determination, 2025, DOI: **10.5517/ccdc.csd.cc2c57b4**; (*d*) CCDC 2179518: Experimental Crystal Structure Determination, 2025, DOI: **10.5517/ccdc.csd.cc2c4z1k**; (*e*) CCDC 2466308: Experimental Crystal Structure Determination, 2025, DOI: **10.5517/ccdc.csd.cc2nsdb6**; (*f*) CCDC 2466313: Experimental Crystal Structure Determination, 2025, DOI: **10.5517/ccdc.csd.cc2nsdhc**; (*g*) CCDC 2466307: Experimental Crystal Structure Determination, 2025, DOI: **10.5517/ccdc.csd.cc2nsd95**.